

Cite this: *J. Mater. Chem.*, 2011, **21**, 15981

www.rsc.org/materials

PAPER

Preparation of PVP coated Cu NPs and the application for low-temperature bonding†

Yan Jianfeng,^a Zou Guisheng,^a Hu Anming^{*b} and Y. Norman Zhou^b

Received 12th May 2011, Accepted 9th August 2011

DOI: 10.1039/c1jm12108a

There is an increasing interest in developing a low temperature interconnection process using nanoparticles. Some studies focus on bonding using Ag nanoparticles (Ag NPs). However, few studies investigate a bonding process using Cu nanoparticles (Cu NPs) due to the easy oxidation in air. Here we achieve a robust bonding of Cu wires to Cu pads with polyvinylpyrrolidone (PVP) coated Cu NPs at a low temperature of 170 °C. The PVP coating can effectively prevent the oxidation of Cu NPs when heated in air. The bonding is formed through the sintering of Cu NPs and direct metallic bonding between the sintered Cu particles and Cu pads. Electrical measurements of the Cu NPs demonstrate that Cu NPs have a low resistivity of $8.6 \times 10^{-5} \Omega \text{ cm}$ after being sintered under pressure. This method has the potential to be used in the electrical packaging industry due to its economic cost, easy operation, and high conductivity.

Introduction

There has been an increasing requirement to develop a low temperature bonding interconnection process in recent years by means of nanojoining technology.¹ Nanojoining, especially nanoscopic diffusion bonding using metallic nanoparticles, has significant advantages over conventional soldering or adhesive bonding. Firstly, this low temperature interconnection technology has potential application for flexible electronics, including flat-panel displays, organic electronics, and low-cost disposable microelectronic devices on a plastic substrate.^{2–4} Secondly, this advanced bonding technology, which allows a lower temperature process, can serve in a higher temperature environment.⁵ This point makes them suitable for applications such as higher power chips and automotive electronics and high power electronic devices, frequently working at a temperature

near 473 K.^{5,6} Moreover, they are lead-free bonding materials which will not bring pollution to the environment and do harm to human health.^{7,8}

There are some investigations about preparing and bonding using Ag or Au nanoparticles.^{9,10} Ide *et al.* have reported a bonding process using Ag nanoparticle paste which was prepared by mixing an organic solvent with the nanoparticles at a temperature of 300 °C.¹¹ Alarifi *et al.* reported bonding of Cu wires at temperatures below 250 °C using Ag NPs.¹² Hu's work confirmed that the sintered network of Ag NPs can work as bonding structures for Cu wires at 100 °C.⁴ Zou *et al.* reported that both Ag nanoparticle paste and powder can be used to bond the silver plated Cu substrates.¹³ Bakhishev and Subramanian investigated the gold nanoparticle inks for lead-free packaging applications.¹⁴

However, these Ag or Au NPs have some shortages. For example, Ag ion migration at relatively high-temperature and humidity conditions will degrade the service life. Au and Ag are expensive. This will restrict their wide application. In contrast, Cu NPs can be used as a perfect material for microscale bonding due to their cheap price and high conductivity.

Several methods have been developed for the preparation of Cu NPs. Lisiecki *et al.* prepared Cu NPs in an aqueous solution in a glove box to prevent the oxidation of Cu NPs, using sodium dodecyl sulfate as capping molecules.¹⁵ B. K. Park *et al.* reported the synthesis of Cu NPs by a polyol method in ambient atmosphere.¹⁶ However, there are few reports on bonding using Cu NPs. The reasons are given as follows: (1) Cu NPs are found to aggregate severely without proper protection; (2) Cu NPs are easily oxidized in air. Actually, it is even difficult to find a simple way to synthesise stable Cu NPs (usually under inert gas environment). Although the problem of oxidation may be suppressed

^aDepartment of Mechanical Engineering & Key Laboratory for Advanced Manufacturing by Materials Processing Technology, Ministry of Education of P. R. China, Tsinghua University, Beijing, 100084, China

^bCentre of Advanced Materials for Joining, Department of Mechanical and Mechatronics Engineering, University of Waterloo, 200 University Avenue West, Waterloo, ON, N2L 3G1, Canada. E-mail: a2hu@mecheng1.uwaterloo.ca; Fax: +1 519-888-6197; Tel: +1 519-888-4567 ext. 35464

† Electronic supplementary information (ESI) available: XPS of Cu NPs: the peaks from (a) C1s, (b) O1s, (c) N1s, and (d) Cu2P3. The different samples of Cu NPs (from bottom to top): samples: (1) Cu NPs with a thin organic shell, (2) Cu NPs with thick polymer coating, (3) Cu NPs with a thin organic shell after heating at 250 °C for 30 min, and (4) Cu NPs with thick polymer coating after heating at 250 °C for 30 min (Fig. S1). Raman spectra of Cu NPs and PVP: (a) Cu NPs with a thin organic shell, (b) Cu NPs with thick polymer coating after heating at 250 °C for 30 min, (c) Cu NPs with a thin organic shell after heating at 250 °C for 30 min, and (d) solid PVP (Fig. S2). SEM (a) and TEM (b–d) images of the typical cross-section of the joints using Cu NPs (Fig. S3). See DOI: 10.1039/c1jm12108a

in vacuum this makes the processing more complicated. Bonding using Cu nanoparticles in air is still a challenge.

In this research, we synthesized the PVP coated Cu NPs by a polyol method in ambient atmosphere. The PVP coating can protect the oxidation of Cu NPs when heated in air. Furthermore, the bonding process using the PVP coated Cu NPs was conducted. The bonding strengths were evaluated by the shear strength test. The bonding mechanism was analyzed using SEM and TEM. To our knowledge, this is the first successful trial of the bonding process using Cu NPs without a protection atmosphere at low temperatures.

Experimental

All the chemicals and reagents were of analytical grade and used as received. Polyvinylpyrrolidone (PVP.K-25) was used as a protecting agent. Sodium hypophosphite monohydrate ($\text{NaH}_2\text{PO}_2 \cdot \text{H}_2\text{O}$) was used to reduce copper nitrate pentahydrate ($\text{Cu}(\text{NO}_3)_2 \cdot \text{H}_2\text{O}$, Sigma-Aldrich). Copper(II) nitrate ($\text{Cu}(\text{NO}_3)_2 \cdot 3\text{H}_2\text{O}$), polyvinylpyrrolidone (PVP.K-25), and sodium hypophosphite monohydrate ($\text{NaH}_2\text{PO}_2 \cdot \text{H}_2\text{O}$) were all purchased from Sigma-Aldrich.

Cu NPs were prepared in a polyol solution using a method modified from the literature.^{16,17} In the polyol method, 2.5 g PVP and 4 g sodium hypophosphite were mixed with 40 ml ethylene glycol (EG, Fisher Chemical) inside a round-bottom flask. The mixture was heated to 90 °C at a rate of 5 °C min^{-1} . Then, 10 ml of 1 M solution of copper nitrate in ethylene glycol liquid at 90 °C was added into the PVP/sodium hypophosphite solution while stirring vigorously. As reduction occurred, the color of the suspension turned from blue to henna within 4–5 min, indicating the formation of Cu NPs. These Cu NPs were concentrated by centrifugation. The clean solvent was extracted from the centrifuge pipes using a pipette, and then the highly concentrated Cu NPs were achieved. Excess PVPs could be removed by washing with deionized (DI) water and centrifugation repeatedly. Cu NPs after washing still had a thin organic shell on the surface, which will be discussed later.

UV-NIR measurements were performed with a Mandel UV-2501 PC spectrometer. Raman spectra were obtained by a microscopic confocal Raman spectrometer (Renishaw, England). The excitation wavelength of the Raman spectra was 514 nm. Thermogravimetry (TGA) and differential scanning calorimetry (DSC) were carried out on a computer controlled NETZSCH 409 PC (Netzsch, Selb, Germany) thermal analyzer. The temperature range was 25–400 °C and the heating rate was 10 °C min^{-1} . Scanning electron microscopy (SEM) measurements were performed with a LEO 1550 field-emission scanning electron microscopy (Zeiss, Oberkochen, Germany). For transmission electron microscope (TEM, JEOL 2010F), the operating voltage is 200 kV. TEM samples were fabricated by dripping Cu NPs onto a carbon film coated Cu grid. The cross-sectional sample was obtained by microtomy. X-Ray diffraction analyses of Cu NPs were recorded at a scanning rate of 0.02° S^{-1} in the 2θ range of 30–80° using a X-ray powder diffractometer (Philips PW 1800, PANalytical Almelo,) with Cu $K\alpha$ radiation ($\lambda = 0.15418$ nm) at 40 kV and 30 mA. The surface chemical states and compositions of the Cu NPs were investigated by X-ray photoelectron spectroscopy (XPS, PHI Quantera, ULVAC-PHI,

Japan) with a monochromatic Al $K\alpha$ 1486.6 eV X-ray source. The spectrometer was calibrated by C1s (BE of 284.8 eV) with respect to the Fermi level.

The specific electrical resistance of Cu NPs was calculated from bulk resistivity of a specimen with specific dimensions. The formulated Cu NPs were coated on a pre-cleaned alumina wafer. The sample was preheated at the temperature of 80 °C for solidification. The width and length of specimen were measured by a digital caliper. The gap between two wafers was adjusted to be 500 μm . Then the sample was annealed under a pressure of 5 MPa. After thermal curing, bulk resistance (R) of paste strips was measured by the digit NanoVolt/Micro-Ohm meter (34420A). Bulk resistivity, ρ , was calculated using the equation

$$\rho = \frac{t \times w}{l} \times R \quad (1)$$

where l , w and t are the length, width and thickness of the sample, respectively. R is the electrical resistance.

The bonding process using Cu NPs was conducted in air. The concentrated Cu NPs were dropped onto the copper pads using a pipette. Then the wires were put on the top of the pads after enough Cu NPs were gathered. Afterwards, these prepared bonding specimens were heated up to the bonding temperature in air under a bonding pressure of 5 MPa, which was measured using a load cell.^{4,12}

The bonding strength was evaluated as shear strength measured using a shear strength test machine (Instron) with a displacement speed of 5 mm min^{-1} at room temperature. The tensile shear strength was calculated by dividing the maximum force by the area of the bond.

Results and discussion

Characteristics of Cu nanoparticles

UV-NIR absorption spectra at various reaction times were used to track the reaction process. Fig. 1 shows the variation of the UV-NIR absorption spectra of the reaction solution taken from the beaker at various times from 0 to 5 min (after adding the copper nitrate in ethylene glycol to the PVP/sodium hypophosphite solution). The characteristic absorption peak at

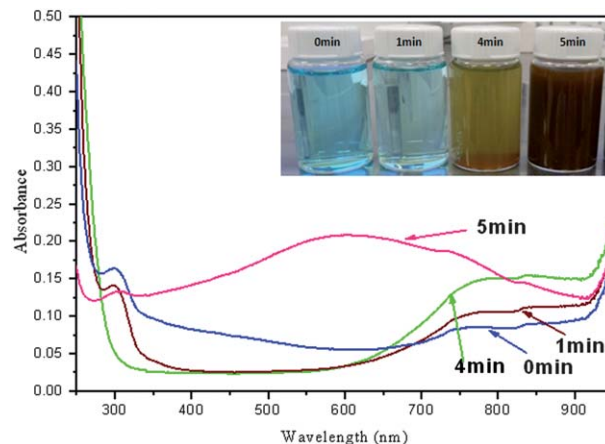


Fig. 1 UV-NIR absorption spectra of copper nanoparticles (solutions were taken from the beaker at various reaction times from 0 to 5 min).

around 575 nm is obvious when the reaction time is 5 minutes. This characteristic absorption peak at around 575 nm is due to the surface-plasmon band of Cu colloids, which is consistent with that of copper nanoparticles synthesized by other methods.¹⁸ This indicates that the copper nanoparticles are formed in 5 minutes after the addition of copper nitrate to the PVP/sodium hypophosphite solution. The broadness of the absorption band probably arises from the wide size distribution of copper nanoparticles.

The mechanism of metal reduction by hypophosphite ions has been described by various schemes.¹⁶ The copper ions may be reduced by atomic hydrogen evolving from the reaction of hypophosphite with water, as the following chemical reactions:

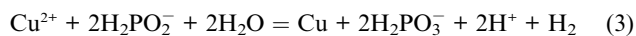
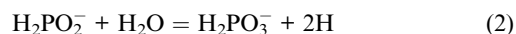


Fig. 2 displays SEM and TEM images of Cu NPs synthesized by the polyol method. When preparing the SEM and TEM samples, the prepared Cu NPs were washed by DI water before being dripped onto the silicon substrate and carbon coated Cu grid. The Cu NPs have a size distribution ranging from 20 to 110 nm and the average diameter is 40.4 nm, after statistically measuring over 100 particles.

From the TEM images, both the spherical Cu NPs and polyhedral Cu NPs are found. The organic shell is clearly viewed. The results also show that the thickness of the organic shell can be controlled by alternatively washing with deionized (DI) water and centrifugation. The constitution of the surface shell is identified by X-ray photoelectron spectroscopy (XPS). Table 1 displays the surface element composition of different Cu nanoparticles. PVP can be identified although the atomic ratio of N/O is lower than the nominal stoichiometric ratio. The difference may be attributed to surface adsorption of other organic groups and/or inner CuO formed between the outer shell and Cu core. It is clear that PVP coating can prohibit the oxidation of Cu NPs. Furthermore, the scanning curve in the vicinity of the C1s (ESI, Fig. S1†) line can be deconvoluted into 4 peaks: 284.5 eV (C–H bonding), 285.3 eV (C–C bonding), 286.2 eV (C–N bonding) and 287.9 eV (C=O bonding). These analyses are consistent with the PVP chemical bonds.¹⁹ The O1s line (ESI, Fig. S1†) comprises two peaks: one at 531.2 eV (C=O bonding) and the other at 533.2 eV (C–OH bonding), indicating the strong chemisorption of PVP to the Cu surface. It has long been known that the final shape of nanoparticles depends on the competitive growth of different crystalline planes and the adsorption of polymer can vary the growth speed of the certain plane. Since the polyvinylpyrrolidone (PVP) has the stabilizing effect in

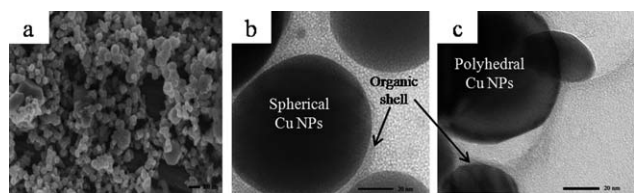


Fig. 2 Morphologies of Cu NPs: (a) SEM image, (b) TEM image of spherical Cu NPs and (c) TEM image of polyhedral Cu NPs.

Table 1 Surface element composition of Cu NPs as detected with XPS: (a) Cu NPs with a thin organic shell, (b) Cu NPs with thick polymer coating, (c) Cu NPs with a thin organic shell after heating at 250 °C for 30 min, and (d) Cu NPs with thick polymer coating after heating at 250 °C for 30 min

Sample	Element concentration (atom%)			
	C1s	N1s	O1s	Cu2P3
a	51.07	9.17	19.20	20.57
b	67.00	8.10	20.86	4.03
c	31.19	4.38	35.59	28.84
d	70.23	11.72	17.93	0.12

preparing Cu nanoparticles by coordination with copper through C–N and C=O bonds, the different morphology may be due to the difference of the concentration of PVP and other ions in the solution during the reaction.^{20,21} Even after washing, some thin organic shell surrounding the Cu NPs can be seen from the TEM images. This thin organic shell prevents the oxidation of synthesized Cu nanoparticles at a temperature lower than 140 °C.

Thermal and oxidation behaviors of Cu NPs

The precondition of using Cu NPs for bonding is to solve the problem of oxidation. The investigation of thermal and oxidation behaviors of Cu nanoparticles is thus necessary. In order to further elucidate the function of the polymer coated on the Cu NPs, thermal analysis of two kinds of Cu NPs was conducted with a heating rate of 10 °C min⁻¹ in air.

Fig. 3 shows the TG and DSC curves of Cu nanoparticles without thick PVP protection (after washing by DI water) and with thick PVP protection (without washing). As shown in Fig. 3a, for Cu nanoparticles without thick PVP protection, the weight loss is observed at the first stage. An exothermic peak is identified at the temperature near 140 °C, and the weight decreases at the same temperature. This may be attributed to the evaporation of the remaining solvent. Based on the above discussion (as shown in Fig. 2), the thickness of PVP is very thin after washing. This results in a slow oxidation of Cu nanoparticles at a temperature above 150 °C. There is a small exothermic peak between 330 and 400 °C, which can be attributed to decomposition of PVP.

Fig. 3b shows TG and DSC curves of Cu NPs with thick polymer protection. It is obvious that no exothermic peak or

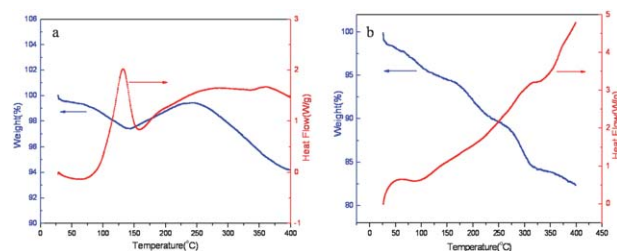


Fig. 3 Thermal analysis of the two kinds of Cu NPs (in air atmosphere, 10 °C min⁻¹): (a) Cu NPs without thick polymer protection and (b) Cu NPs with thick polymer protection.

endothermic peak is detected at a temperature less than 300 °C. Meanwhile the weight decreases gradually. This indicates that no remarkable oxidation of Cu NPs happens at this stage. A small exothermic peak around 320 °C corresponds to the decomposition of PVP. From these thermodynamic analyses, it can be concluded that Cu NPs without thick polymer protection will be oxidized when heated at a temperature higher than 140 °C. However, for the Cu nanoparticles with thick polymer protection, no remarkable oxidation happens. This indicates that the PVP coating can protect them from oxidation effectively.

The protection effect of PVP coating can be confirmed by the SEM images and XRD tests (as shown in Fig. 4 and 5). As shown in Fig. 4, no oxides are detected after annealing at 100 °C for 30 min. However, after annealing at a higher temperature of 200 °C, Cu NPs are gradually oxidized into Cu₂O. After annealing at 300 °C, all the Cu NPs are converted to CuO. Since both Cu₂O and Cu are detected after annealing at 200 °C by XRD, this may indicate that when the oxidation of Cu nanoparticles occurs, the surface of Cu changes to Cu₂O and CuO firstly, and then the Cu core is gradually oxidized.²² Besides the coarsening of Cu grains, it is found that the surface of Cu NPs becomes rough when the oxidation takes place. The increase of the surface roughness may be related to the formation of Cu₂O and CuO. The reported results are consistent with the above thermodynamic results which indicate the oxidation occurs above 140 °C. These analyses are also in agreement with the investigation by Raman spectroscopy (as shown in the ESI, Fig. S2†). For coated PVP a peak at 1623 cm⁻¹ can be attributed to the C=N bond with a positive charge on N due to the configuration to Cu through C-O bond.¹⁹ It is worth noting that the 1670 cm⁻¹ peak of the C=O stretch mode of PVP bulk cannot be detected. This indicates that PVP in the coating layer behaves differently from the PVP bulk due to the strong interaction with Cu NPs. However, after heat treating Cu NPs with a thin organic shell at 250 °C for 30 min, 1623 cm⁻¹ peak totally disappears, indicating an evaporation or decomposition of the PVP shell at this temperature.

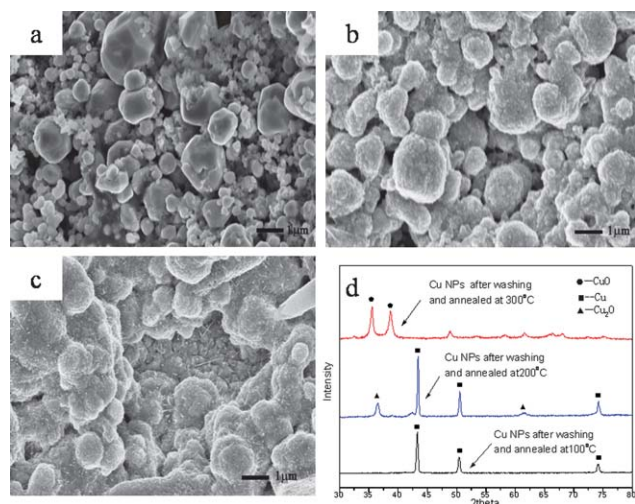


Fig. 4 SEM images (a–c) and XRD patterns (d) of Cu NPs after washing and annealing at 100 °C, 200 °C and 300 °C for 30 min, respectively.

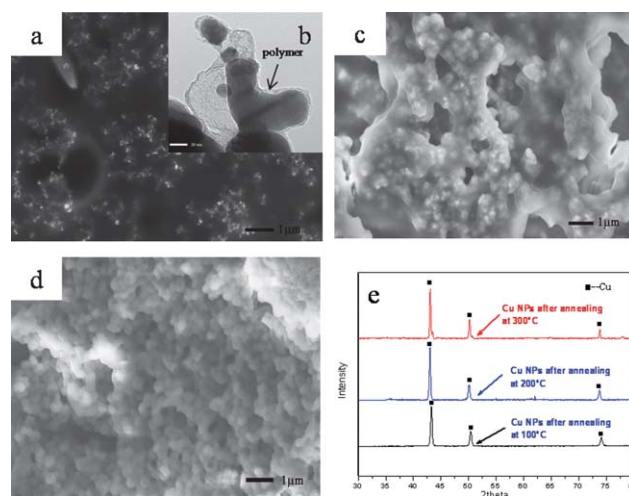


Fig. 5 SEM images (a, c and d), TEM (b) and XRD patterns (e) of Cu NPs coated by the polymer and annealed at 100 °C, 200 °C and 300 °C for 30 min, respectively.

SEM images unveil the same variation. After sintering at 100 °C for 30 min, Cu NPs are surrounded by a lot of PVP and just a few of Cu NPs can be observed by SEM (Fig. 5a). After sintering at 300 °C for 30 min (Fig. 5d), Cu NPs are surrounded by the thinner polymer and more Cu NPs can be seen in close contact with each other. The grain growth of Cu NPs is also confirmed by the calculation from XRD patterns according to the Scherrer equation:

$$D = \frac{K\lambda}{B \cos \theta} \quad (4)$$

where D is the average particle size, K is the Scherrer constant related to the shape and index (111) of the crystals. B is the additional broadening, $\lambda = 0.15418$ nm (Cu K α), and θ is the Bragg angle. The calculated average particle sizes of Cu NPs annealed at 100 °C, 200 °C and 300 °C for 30 min are 34 nm, 41 nm and 100 nm, respectively. Although the calculation value is slightly smaller than statistical values the results illustrate that grain growth occurs when annealed at a higher temperature. From the above discussion, it is evident that the PVP coating can protect the Cu NPs from oxidation and the sintering will occur after the volatilization and decomposition of most of the PVP.

Weldability properties of Cu NPs

Since the PVP can protect Cu NPs from coalescence and oxidation, the current Cu NP paste is a promising material for microelectronics interconnection. Fig. 6 shows the tensile strength of the bonded Cu wires to Cu pads with Cu NPs at a pressure of 5 MPa plotted against sintering temperatures. At the bonding temperature of 160 °C, the shearing strength is low (~1 MPa). By slightly increasing the temperature to 170 °C, the strength can be enhanced dramatically. At the bonding temperature of 220 °C, the Cu wires are broken. The fracture position is the Cu wire instead of the joint area, indicating the formation of a strong metallurgical bond.

Compared to the reported results in which Ag metallo-organic compounds are used to bond Cu pellet to pellet, the shear

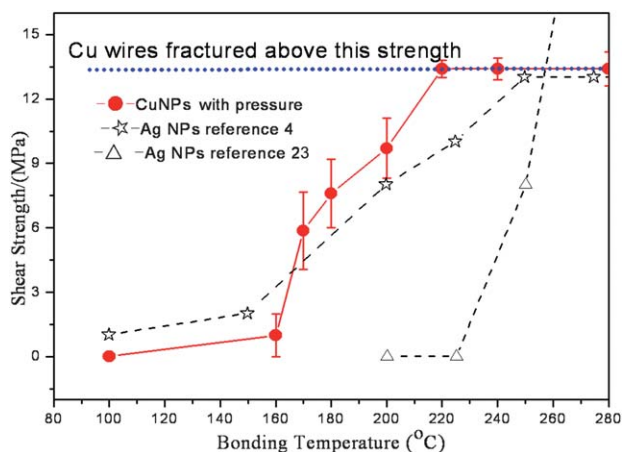


Fig. 6 Tensile strength of bonded Cu wires to Cu pads with Cu NPs as a function of sintering temperatures (data in ref. 4 are from Hu's paper and data in ref. 23 are from Akada's paper).

strengths using Cu NPs are much higher.²³ The bonding of Cu wires to Cu pads with Ag NPs is also displayed in Fig. 6 for comparison.⁴ It can be seen that the shear strength of the joints using Cu NPs is even higher than that using Ag NPs at temperatures higher than 160 °C. From the above analysis, it can be seen that the joints using Cu NPs are comparable or better than those using Ag NPs or Ag metallo-organic compounds. Since Cu is much cheaper than Ag, the present results display a great advantage using Cu NPs for microelectronics packaging and interconnection.

The typical fracture surfaces of the joints bonded using Cu NPs at different temperatures are shown in Fig. 7. Different fracture microstructures are formed when bonded at different temperatures. At the bonding temperature of 160 °C, isolated Cu NPs spread between the Cu wires and pads. No obvious necks are formed and this may cause the low bonding strength at this temperature. As the temperature is increased to 220 °C, the neck is formed between adjacent particles. This may lead to the

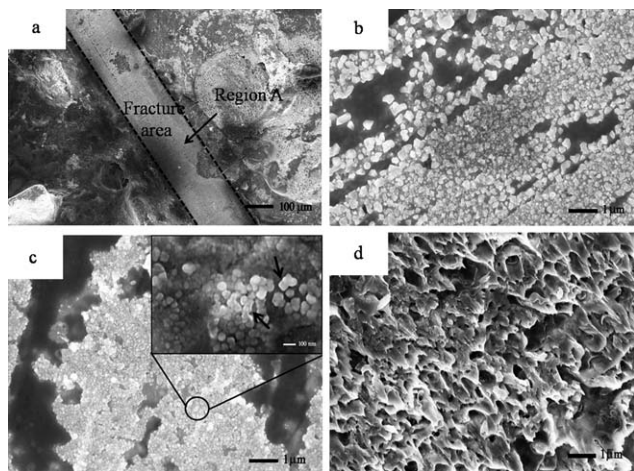


Fig. 7 SEM images of a typical fracture surface of joint using Cu NPs at different temperatures. (a) Lower magnification image and higher magnification images at regime A at different temperatures: (b) 160 °C, (c) 220 °C, and (d) 280 °C.

increase of the shear strength. At the bonding temperature of 280 °C, dimple microstructures are observed, indicating that sintered Cu NPs have some ductile characteristics at higher temperatures.²⁴

SEM images of the cross-section of the joint show that the Cu wire and pad are joined together closely (as shown in Fig. S3(a)† in the ESI). No crack was detected by SEM observation. Based on the TEM images (Fig. S3(b–d)† in the ESI), the sintered Cu nanoparticles form micro-scale Cu grains. Moreover, the TEM images confirm that the metallic bond is achieved at the interface between the sintered Cu layer and both sides of the joint without a distorted layer. This result is similar to the TEM observations when bonding Cu wires and pad using Ag NPs.¹² But this result is different from the bonding with Ag NPs obtained through the decomposition of metallo-organic compounds.^{11,27} When bonding through the decomposition of metallo-organic compounds, a distorted layer of 1–3 nm thickness was observed between Cu and Ag. The current TEM observation shows an enhanced match between the Cu–Cu interfaces. This improved match between Cu NPs and Cu substrate may be the reason that a stronger joint using Cu NPs is achieved than that using Ag NPs, as shown in Fig. 6.

In most cases, the incorporation of metal nanoparticle into a polymer matrix will result in a polymer composite with high resistivity.^{25,28–30} The reasons are twofolds:²⁵ the difficulty of debonding or decomposition of organic molecules^{31,26,32} and the impediment of the sintering of nanoparticles by high fraction of highly cross-linked polymer matrices.²⁶ The increased contact points and contact area among conductive fillers will reduce the resistivity.²⁹ Thus it remains a challenge to achieve highly conductive polymer composites through the sintering of nanoparticles. In the current study, we find that the assistance of pressure is necessary to improve the resistivity of PVP coated Cu NP materials. The resistivity of Cu NPs after sintering in air without pressure is in a range of a few hundred kΩ. However, by sintering at a pressure of 5 MPa, the conductivity of sintered Cu is improved significantly. Fig. 8 shows the bulk resistivity of Cu NPs paste after sintering under 5 MPa for 30 min at different temperatures. After curing at 200 °C, the Cu NPs show a high resistivity ($1.1 \times 10^{-3} \Omega \text{ cm}$). By elevating the curing temperature

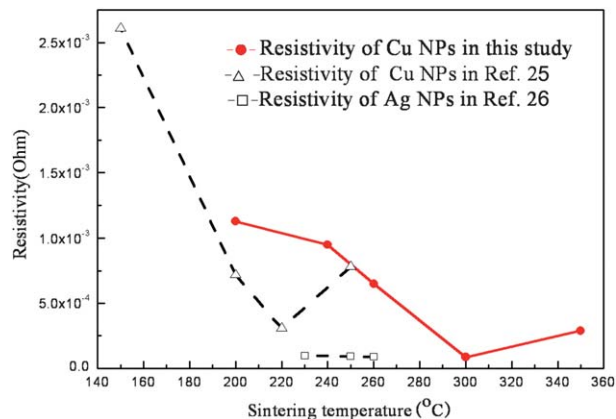


Fig. 8 Bulk resistivity of Cu NPs paste after sintering for 30 min at different temperatures (data in ref. 25 are from Pulkkinen's paper and data in ref. 26 are from C. P. Wong's paper).

to 240 °C and 260 °C, the resistivity decreases to $9.5 \times 10^{-3} \Omega \text{ cm}$ and $8 \times 10^{-3} \Omega \text{ cm}$, respectively. As the temperature increases to 300 °C, the sintered Cu NPs yield a low resistivity ($8.6 \times 10^{-5} \Omega \text{ cm}$). It should be noted that this value is very close to that of polymer nanocomposites cured using typical lead-free solder reflow profiles ($6.3 \times 10^{-5} \Omega \text{ cm}$).^{30,33} The decrease of resistivity with the increase of curing temperature may be due to the sintering of Cu NPs after decomposition of the polymer at elevated temperatures. However, the resistivity increases to $2.9 \times 10^{-4} \Omega \text{ cm}$ at a temperature of 350 °C. This may be caused by the oxidation of Cu NPs at this temperature. This electrical resistivity is still low in comparison with the reported data.^{25,26} According to SEM and TEM images (Fig. 7 and S3†), it is reasonable to conclude that the sintering of the Cu NPs results in the enhancement of conductivity.

Conclusions

In summary, we have developed a route to prepare the PVP coated Cu NPs and a low temperature bonding process using PVP coated Cu NPs in ambient atmosphere. The PVP coating can protect the oxidation of Cu NPs when heated in air. The shearing test shows that the joint strength using Cu NPs is better than that using Ag NPs. Based on the fracture surfaces and cross-sectional analysis, it is found that a metallurgical connection is formed between the base metal and Cu NPs. The isolated Cu NPs are converted to the micro-scale connected Cu grains. Electrical measurements of the Cu NPs demonstrate that after sintering at a pressure of 5 MPa, Cu NPs yield a low resistivity of $8.6 \times 10^{-5} \Omega \text{ cm}$. To our knowledge, this is a systematic study with Cu NPs processed in air down to 170 °C. The method developed here has the potential to be used in electrical packaging industry and plastic electronics.

Acknowledgements

This research is partially supported by the National Natural Science Foundation of China (grant no. 51075232), Tsinghua University Initiative Scientific Research Program (grant no. 2010THZ 02-1), Canada Research Chair fund, and National Science and Engineering Research Council (NSERC, Canada) discovery grant.

Notes and references

- 1 Y. ZHOU, *Microjoining & Nanojoining*, Woodhead Publishing Ltd, CRC Press, England, 2008.
- 2 Q. Cui, F. Gao, S. Mukherjee and Z. Gu, *Small*, 2009, **5**, 1246–1257.

- 3 Y. Lu, J. Y. Huang, C. Wang, S. Sun and J. Lou, *Nat. Nanotechnol.*, 2010, **5**, 218–224.
- 4 A. Hu, J. Y. Guo, H. Alarifi, G. Patane, Y. Zhou, G. Compagnini and C. X. Xu, *Appl. Phys. Lett.*, 2010, **97**, 153117.
- 5 T. Morita, E. Ide, Y. Yasuda, A. Hirose and K. Kobayashi, *Jpn. J. Appl. Phys.*, 2008, **47**, 6615–6622.
- 6 T. G. Lei, J. N. Calata, L. Guo-Quan, C. Xu and L. Shufang, *IEEE Trans. Compon. Packag. Technol.*, 2010, **33**, 98–104.
- 7 Y. Li, K. Moon and C. Wong, *Science*, 2005, **308**, 1419–1420.
- 8 M. Abteu and G. Selvaduray, *Mater. Sci. Eng., R*, 2000, **27**, 95–141.
- 9 J. Kasthuri and N. Rajendiran, *Colloids Surf., B*, 2009, **73**, 387–393.
- 10 Y. Long, J. Wu, H. Wang, X. Zhang, N. Zhao and J. Xu, *J. Mater. Chem.*, 2011, **21**, 4875–4881.
- 11 E. Ide, S. Angata, A. Hirose and K. F. Kobayashi, *Acta Mater.*, 2005, **53**, 2385–2393.
- 12 H. Alarifi, A. Hu, M. Yavuz and Y. Zhou, *J. Electron. Mater.*, 2011, **40**, 1394–1402.
- 13 G. Zou, J. Yan, F. Mu, A. Wu, J. Ren, A. Hu and Y. N. Zhou, *Open Surf. Sci. J.*, 2011, **3**, 70–75.
- 14 T. Bakhishev and V. Subramanian, *J. Electron. Mater.*, 2009, **38**, 2720–2725.
- 15 I. Lisiecki, F. Billoudet and M. P. Pileni, *J. Phys. Chem.*, 1996, **100**, 4160–4166.
- 16 B. K. Park, S. Jeong, D. Kim, J. Moon, S. Lim and J. S. Kim, *J. Colloid Interface Sci.*, 2007, **311**, 417–424.
- 17 Y. Lee, J.-r. Choi, K. J. Lee, N. E. Stott and D. Kim, *Nanotechnology*, 2008, **19**, 1–7.
- 18 M. Abdulla-Al-Mamun, Y. Kusumoto and M. Muruganandham, *Mater. Lett.*, 2009, **63**, 2007–2009.
- 19 D. P. Schweinsberg, G. A. Hope, A. Trueman and V. Otieno-Alego, *Corros. Sci.*, 1996, **38**, 587–599.
- 20 I. Haas, S. Shanmugam and A. Gedanken, *J. Phys. Chem. B*, 2006, **110**, 16947–16952.
- 21 Z. Zhang, B. Zhao and L. Hu, *J. Solid State Chem.*, 1996, **121**, 105–110.
- 22 D. B. Pedersen, S. Wang and S. H. Liang, *J. Phys. Chem. C*, 2008, **112**, 8819–8826.
- 23 Y. Akada, H. Tatsumi, T. Yamaguchi, A. Hirose, T. Morita and E. Ide, *Mater. Trans.*, 2008, **49**, 1537–1545.
- 24 A. Hasnaoui, H. Van Swygenhoven and P. M. Derlet, *Science*, 2003, **300**, 1550–1552.
- 25 P. Pulkkinen, J. Shan, K. Leppänen, A. Käsäkoski, A. Laiho, M. Järn and H. Tenhu, *ACS Appl. Mater. Interfaces*, 2009, **1**, 519–525.
- 26 R. Zhang, K.-s. Moon, W. Lin and C. P. Wong, *J. Mater. Chem.*, 2010, **20**, 2018–2023.
- 27 T. Morita, E. Ide, Y. Yasuda, A. Hirose and K. Kobayashi, *Jpn. J. Appl. Phys.*, 2008, **47**, 6615.
- 28 H.-H. Lee, K.-S. Chou and Z.-W. Shih, *Int. J. Adhes. Adhes.*, 2005, **25**, 437–441.
- 29 Y. Lilei, L. Zonghe, L. Johan and A. Tholen, *IEEE Trans. Compon. Packag. Technol.*, 1999, **22**, 299–302.
- 30 R. Zhang, W. Lin, K.-s. Moon and C. P. Wong, *ACS Appl. Mater. Interfaces*, 2010, **2**, 2637–2645.
- 31 B. J. Perelaer, A. W. M. de Laet, C. E. Hendriks and U. S. Schubert, *J. Mater. Chem.*, 2008, **18**, 3209–3215.
- 32 D. Untereker, S. Lyu, J. Schley, G. Martinez and L. Lohstreter, *ACS Appl. Mater. Interfaces*, 2009, **1**, 97–101.
- 33 H. Jiang, K.-s. Moon, Y. Li and C. P. Wong, *Chem. Mater.*, 2006, **18**, 2969–2973.